DOE/ET/13384-T2

SOLID CIRCULATION AROUND A JET IN A FLUIDIZED-BED GASIFIER

Final Report

Hugo S. Caram
Babu Patrose

Lehigh University
Bethlehem, PA 18015

Date Published - April 1981

Prepared for the United States
Department of Energy

Under Contract No. DE-FG21-78ET13384

DISCLAIMER

SOLID CIRCULATION AROUND A JET IN A FLUIDIZED-BED GASIFIER

Final Report

Hugo S. Caram
Babu Patrose

Lehigh University
Bethlehem, PA 18015

Date Published - April 1981

Prepared for the United States
Department of Energy

Under Contract No. DE-FG21-78ET13384

Printed in the United States of America

Available from

National Technical Information Service
U. S. Department of Commerce
5285 Port Royal Road
Springfield, Virginia 22161

CONTENTS

ABSTRACT

The research described in this report was carried out at Lehigh University through the U.S. Department of Energy Contract No. DE-FG21-78ET13384. The main purpose of the study was the analysis of particle circulation in the jet region of a fluidized bed gasifier. The two fundamental questions answered by this report relate to the measurement of particle velocities in the grid region and to the relevance of the jet zone to the operation of the reactor.

A compact optical fiber probe to measure the velocity of solid particles in two-phase flows was constructed. The probe has been used to measure particle velocities and obtain flow trajectories of solids in the distributor grid region of a two-dimensional fluidized bed. Air was used as the fluidizing medium in a bed of glass beads of size ranging from 0.2 to 0.7 mm.

Particle velocities were measured at corresponding points within a jet in the two-dimensional bed, using the optical fiber probe and a Laser Doppler Velocimeter (LDV). The probe measurements compare well with the LDV results in the main jet region. Particle velocities were also measured with the probe in the dense phase region of the fluidized bed where measurements were not possible using LDV. The resulting flow maps clearly indicate solids circulation patterns around jets and identify dead zones formed on the distributor plate.

The entering gas jet was modeled assuming that the dense phase is entrained into the gas stream. The solid particles are then conveyed upwards along the jet penetration distance. Typical conditions for a fluidized bed combustor were used and the model includes the reactions between carbon and carbon dioxide and oxygen and the homogeneous oxidation of carbon monoxide. The results indicate that considerable reaction occurs in the gas jets entering the reactor and that they should be considered in any careful analysis of its operation.

CHAPTER 1

AN OPTICAL FIBER PROBE FOR PARTICLE VELOCITY MEASUREMENTS IN FLUIDIZED BEDS

The proper design of the distributor has been identified as the key to the successful operation of a fluidized bed reactor (Wen and Dutta, 1977). Many investigators have indicated that gas and solid contacting is more efficient near the grid than higher up in the bed. Further, the distributor design greatly influences the physical and chemical performance of the bed (Bottom, 1970; Behie and Kehoe, 1973; Cooke et al., 1968).

Much qualitative information can be found on the importance and nature of gas and solids mixing in the grid region. However, very little quantitative information has been reported to adequately describe the flow characteristics of gas and solids in the region close to the grid plate.

A schematic representation of possible gas and solids flow patterns near the grid region is shown in Figure 1.1. It is our objective to study the effects of operating variables on the structure of the jet, the solid circulation patterns and dead zone formation in this region. The design and application of the optical fiber transit anemometer for particle velocity measurement are described. The optical fiber probe was used to measure particle velocities in a two-dimensional fluidized bed using the transit time correlation technique. The probe is small in size and its insertion into a flow would result in minimal interference. The use of the probe does not require apriori knowledge of the flow orientation, nor does it require alignment or orientation along the direction of flow. However, the probe requires calibration and a dual beam LDV was used as the standard for calibration.

TWO-PHASE FLOW MEASUREMENT TECHNIQUES

Techniques available for two-phase flow measurement are those based on impact, thermal, electrical, optical and photographic methods.

In the impact strain gage probe a piezoelectric crystal converts the strain on the probe into an electrical signal s, such that

$$\rho_s U_p = k \varepsilon s$$

The local particle velocity can therefore be calculated, provided the local bed porosity is known (Heertjes et al., 1970;

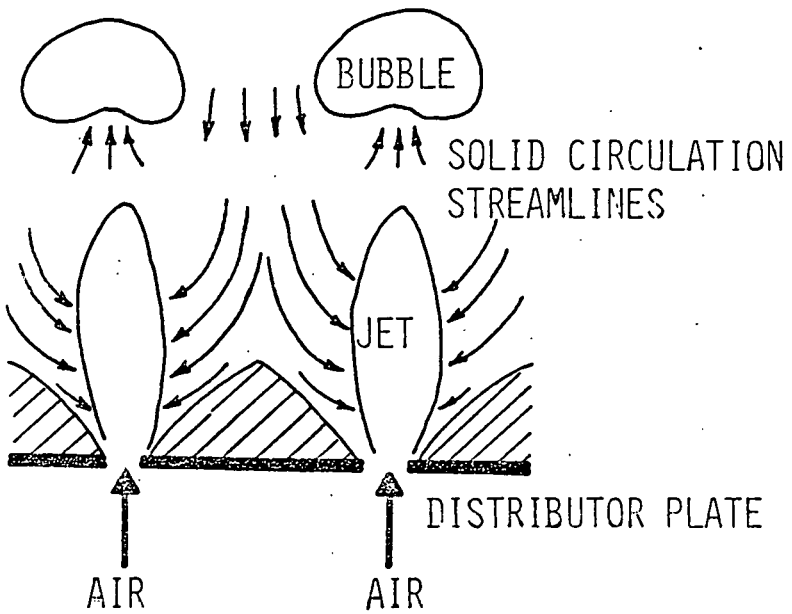

Figure 1.1: Schematic representation of solids flow pattern and dead zone formation in the grid region. After Wen and Dutta (1977).

Livshits and Tamarin, 1979). However, it is difficult to simultaneously measure local bed porosity and the magnitude of the signal (Oki et al., 1977). Donadono et al. (1980) and Donsi et al. (1980) used impact probes to determine the number of particles flowing per unit time through the jet cross section in a fluidized bed. Local solids volume concentration was obtained using this information together with the average particle velocity measured using high speed photography.

Marsheck and Gomezplata (1965) have reported measurements of local mass flow rate of solid particles in a fluidized bed using a thermistor probe. The probe tip consists of a heating thermistor and a sensing thermistor positioned adjacent to each other. When aligned with the heating thermistor upstream to the sensing thermistor, an increase in flow rate increases the heat transfer rate between the two thermistors. To determine flow direction, the probe must be aligned in such a way that the sensing thermistor indicates a maximum change in its resistance. The probe requires calibration for different types of particles, and its performance depends on the characteristics of the particles and the bed.

Electrical methods employed in two-phase flow measurements usually entail resistance or capacitance measurements. Beck et al. (1968) computed particle velocities in pneumatic conveyors, from the transit time of the naturally occurring noise pattern between capacitor plates at two positions along the axis of the conveyor. The average velocity in the line is then given by

$$U_p = \ell_{AB}/\tau_o$$

The transit time was determined by cross correlating the transducer outputs using an online digital computer. Similar measurements were made using conductivity transducers at two different points in the flow (Beck et al., 1973).

Visual techniques are very convenient to obtain overall particle trajectories, and are of value particularly in systems with particles in transient motion. High speed photography can be used to obtain particle flow patterns and velocities in systems with dilute loading of solid particles (Donadono et al., 1980; Donsi et al., 1980; Donadono and Massimilla, 1978; Knowlton and Hirsam, 1980). Yong et al. (1980) studied particle movement in a two-dimensional fluidized bed by observing the fluorescent light emitted by ZnS impregnated PMMA particles following laser-induced excitation. They computed particle velocity by dividing the distance between two successive bright fluorescent points by the period of the pulsating laser emission. Latif and Richardson (1972) studied the movement of particles within a

fluidized bed by following the motion of a tracer particle which is typical of the particles making up the bed. Such visual techniques have the advantage of not disturbing the flow, but their application is limited to systems having transparent walls. Individual particles need to be tracked to obtain velocity data. A very large number of such measurements must be made in order to give a statistically significant result making the procedure very tedious.

Laser Doppler Velocimeters (LDV) use the frequency information contained in light scattered by particles passing through an interference fringe pattern to determine particle velocities (Birchenough and Mason, 1976; Lee and Srinivasan, 1977; Morton and Clark, 1971). The LDV is an obstructionless technique and requires no calibration. However, LDV application requires an optical path to the point of measurement. It is therefore well suited for measuring velocities in flow systems with dilute solids loading and cannot be used in the opaque dense phase of a fluidized bed.

The light transmission ability and small size of optical fibers have been the basis for other optical techniques to measure velocity (Hemstrom, 1976; Miller and Mitchie, 1969). Oki et al. (1977) developed an optical fiber probe to measure velocity using the transit time method. It was made of three opitcal fibers with light being transmitted through the central fiber and reflected light from the particles being received through the other two fibers. The time delay between the two signals was computed using a correlator, and the particle velocity was then obtained by dividing the fiber separation distance by the time delay. Shirai et al. (1977) used such a probe to measure particle velocities in the neighborhood of a rotating horizontal disc within a particle bed.

TRANSIT TIME CORRELATION TECHNIQUE

The transit time, τ_o, for a particle to travel between two points, A and B separated by a distance $|\ell_{AB}|$, can be used to compute the velocity component of a flow in the direction of the vector connecting the two points as:

$$U_p = |\ell_{AB}|/\tau_o$$

If signals A(t) and B(t) represent the variation of intensity of the reflected light at two points A and B for a single particle passing through the two points, the transit time can be determined by the delay between the maxima of the signals A(t) and B(t) (Figure 1.2). In a more general case, there will be a large number of particles present, not all of them will pass through both points and it will be difficult

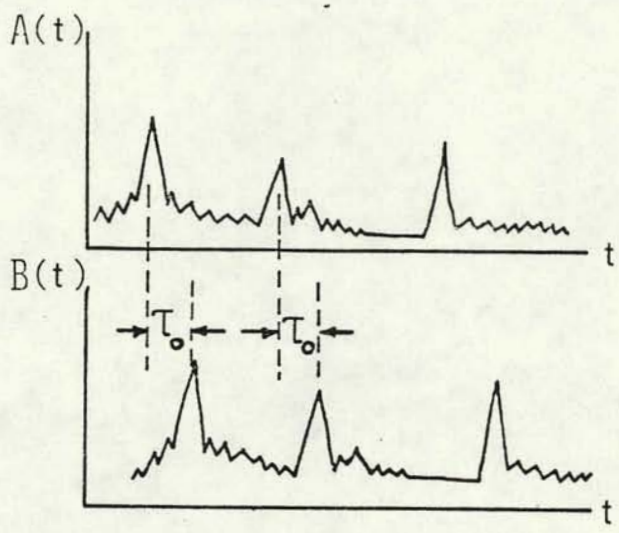

Figure 1.2: Signals fed to the correlator.

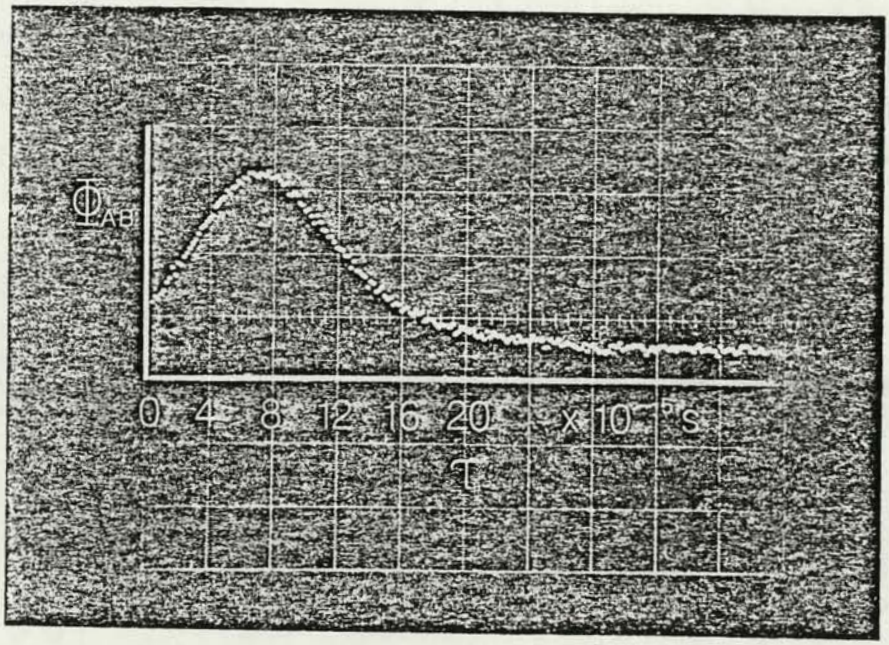

Figure 1.3: The cross-correlation function computed by the correlator. $\Phi_{AB}(\tau) = \frac{1}{T}\int_o^T A(t) \cdot B(t+\tau)\, dt.$

to identify individual particles. However, an average time delay can be obtained from the maximum of the cross-correlation function:

$$\Phi_{AB}(\tau) = \frac{1}{T}\int_{o}^{T} A(t)\ B(t+\tau)\ dt \qquad (1.1)$$

where $T >> \tau_{max}$. This has the advantage of minimizing the influence of random noise. Assuming that the signals contain random noise components $N_A(t)$ and $N_B(t)$, respectively,

$$\Phi_{AB}(\tau) = \frac{1}{T}\int_{o}^{T} \Big[A(t)\ B(t+\tau) + A(t)\ N_B(t+\tau) + N_A(t)\ B(t+\tau) + N_A(t)\ N_B(t+\tau) \Big] dt$$

$$\Phi_{AB}(\tau) \simeq \frac{1}{T}\int_{o}^{T} A(t)\ B(t+\tau)\ dt$$

where the noise frequency is assumed to be high compared to the frequency associated with the particles transit time.

It is also possible to compute the time delay by computing the autocorrelation of the sum of the two signals, [A(t) + B(t)]; but experimental difficulties are encountered because for the small probes used, the duration of the signals collected from individual particles is comparable to the time delay between detection points.

THE OPTICAL FIBER PROBE

The technique described in the previous section can be realized using a fine probe made of optical fibers to transmit the reflected light from points A and B in the flow to photomultipliers that produce voltage outputs that are proportional to the intensity of light signals they receive. Optical fibers are well suited for the purpose because they are available as narrow strands--as small as 50 μm in diameter. It therefore becomes possible to construct fine optical fiber probes which produce only marginal disturbance when introduced into a flow.

The optical fiber probe constructed for this study used five illuminating fibers to achieve a more uniform and intense illumination of the region of the flow field where the measurement is made. To ensure good light transmission and reproducibility of measurements, the fiber tips were polished using 1 μm alumina on a felt polishing wheel.

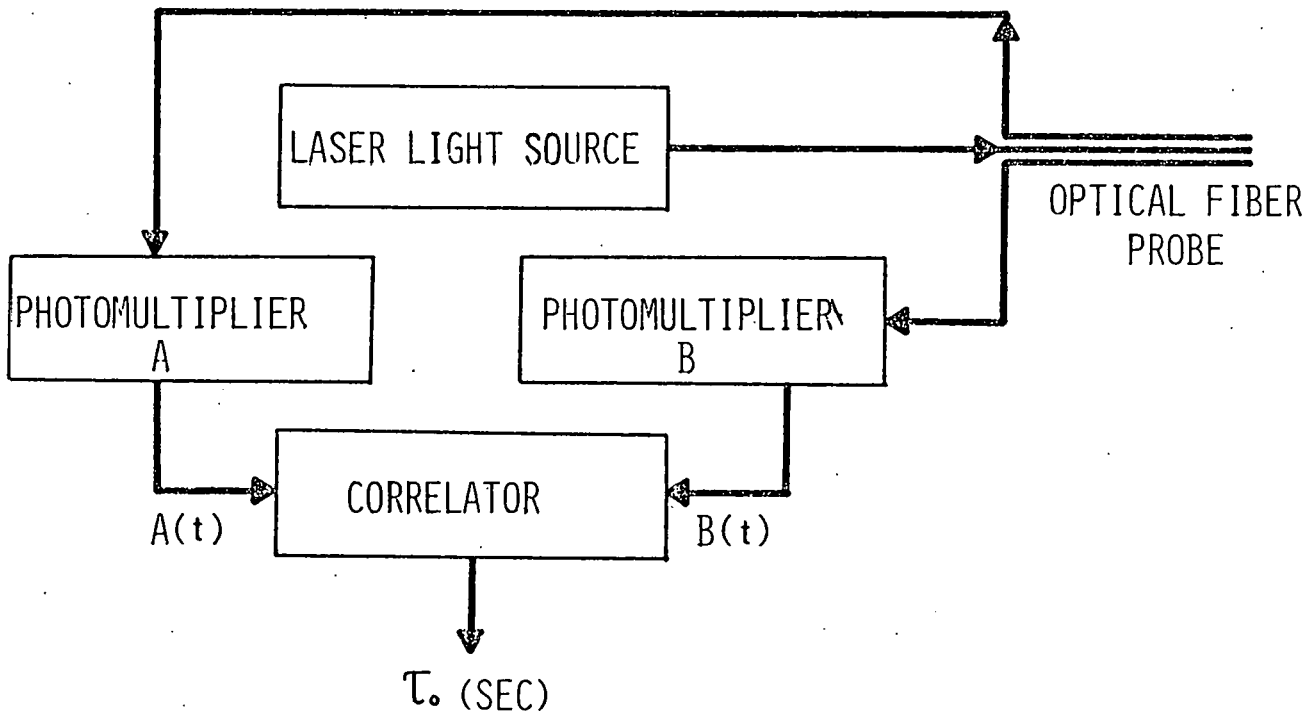

Figure 1.4: Instrumentation and signal flow diagram.

INSTRUMENTATION

The instrumentation block diagram is shown in Figure 1.4. The light source used was a 15 mW He-Ne laser. The variations of reflected light, captured by the receiving fibers in the probe, are converted to electric signals A(t) and B(t) by photomultipliers. These signals are fed to the correlator (Honeywell SAI-43A, correlation and probability analyzer). The computed cross-correlation function given by Equation (1.1) was displayed on an oscilloscope. The time delay τ_o was obtained by reading the location of the maximum of the displayed cross-correlation function (Figure 1.3).

DERIVATION OF EQUATIONS

Figure 1.5 represents a head-on view of the probe where the thick solid line represents the trajectory of a particle moving with velocity U_p at an angle θ to the horizontal. Also shown are the relative variations in intensity of the reflected light captured by the receiving fibers at locations y_1 and y_2. They show a maximum in the reflected light intensity as the particle passes closest to the corresponding fiber. The time delay τ_y between the two maxima is the time taken for the particle moving at velocity U_p to traverse a distance d_y. Therefore,

$$U_p = \frac{d_y}{\tau_y} = \frac{d_x}{\tau_x}$$

where the same analysis has been applied to the signals collected by the fibers located at x_1 and x_2, and delayed by time τ_x.

In practice, τ_x and τ_y are the transit times computed by the correlator using the cross-correlation technique. The magnitude $|U_p|$ and direction (θ) of the flow are determined using the relations

$$U_p = \left[\left(\frac{\tau_y}{\ell_y}\right)^2 + \left(\frac{\tau_x}{\ell_x}\right)^2\right]^{-1/2} \qquad (1.2)$$

and

$$\theta = \text{Arc tan}\left[\frac{\tau_y}{\tau_x} \cdot \frac{\ell_x}{\ell_y}\right] \qquad (1.3)$$

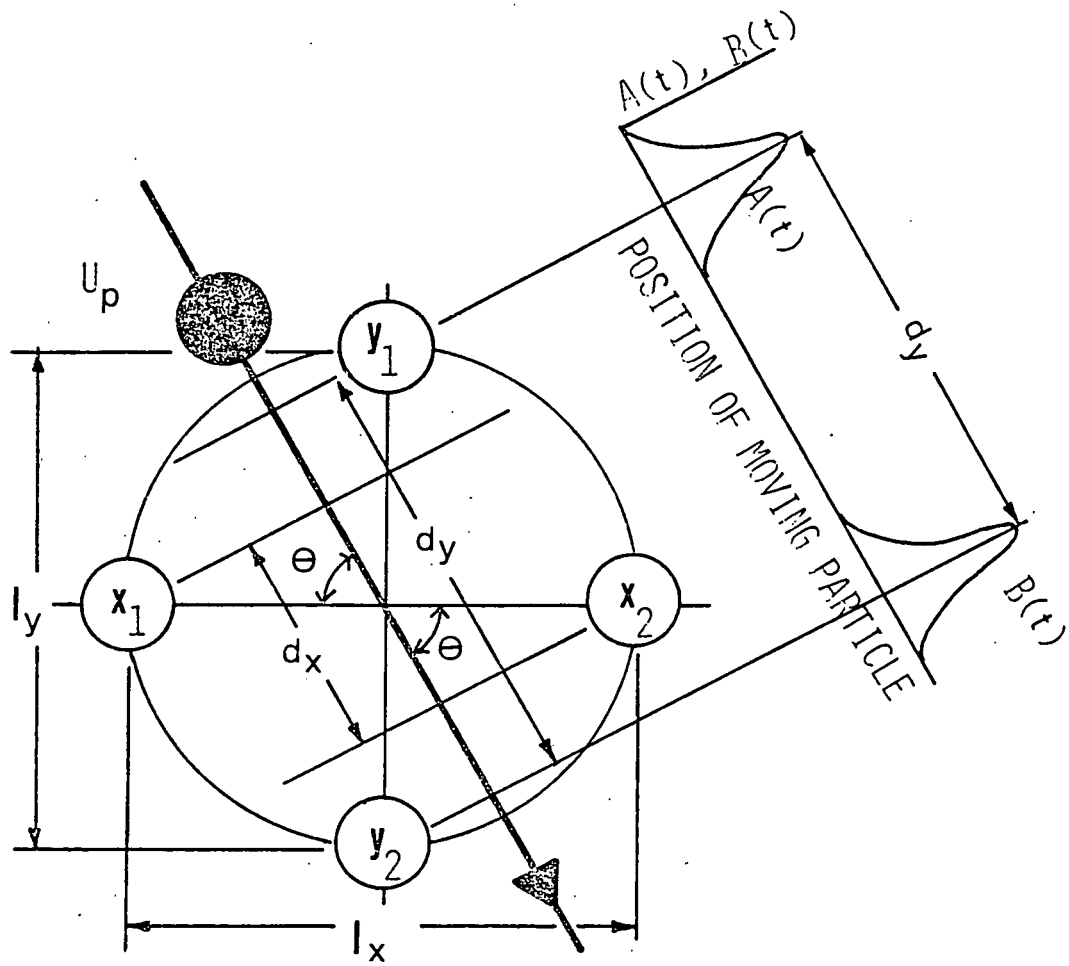

= SOLID PARTICLE MOVING WITH VELOCITY U_p

= RECEIVING OPTICAL FIBER

Figure 1.5: Schematic of the measuring system.

Equations (1.2) and (1.3) specify the magnitude of the particle velocity and its direction, and thereby completely define the projection of the particle velocity vector on the plane perpendicular to the tip of the fiber probe.

Notice that since the sign of the time delay is known from the cross-correlation function, it becomes possible to determine the orientation of the flow, and the directional ambiguity encountered in Laser Doppler Velocimetry is eliminated.

PROBE CALIBRATION

The use of Equations (1.2) and (1.3) requires the knowledge of ℓ_x and ℓ_y, the effective fiber to fiber separation distance. One would intuitively expect the value of ℓ to be used in these equations, to be equal to the actual center to center distance between the receiving fibers. To verify this calibration experiments were performed in a free-falling stream of glass beads (d_p = 500 μm), and the value of ℓ was calculated from the particle velocity measurements made using dual beam Laser Doppler Velocimetry (LDV). Since LDV is an absolute technique, no calibration is required. The free jet configuration was chosen for calibration of the probe because it approximates very closely the two-phase nature of the bed in which the actual particle velocity measurements were made.

Particle velocity measurements were made using dual beam LDV at different locations within the falling stream of particles. At each location the probe was positioned such that its front tip exactly coincided with the measuring volume formed by the two laser beams of the LDV. This ensured that the transit time information obtained from the probe corresponded to the particle velocity measured by the LDV. The particle velocity U_p and the transit time τ_o are used to compute the effective fiber to fiber separation distance ℓ:

$$\ell = U_p \cdot \tau_o$$

Table 1.1 includes a representative set of calibration data. The average effective distance ℓ was found to be 0.14 mm; whereas, the actual geometric center to center distance between the two receiving fibers was measured under the microscope to be 0.37 mm. The 'apparent' or 'effective' distance is seen to be a function of the viewing angle of the receiving fibers and the nature of illumination produced at the measuring site (Figure 1.6). Two extreme cases of illumination are discussed here.

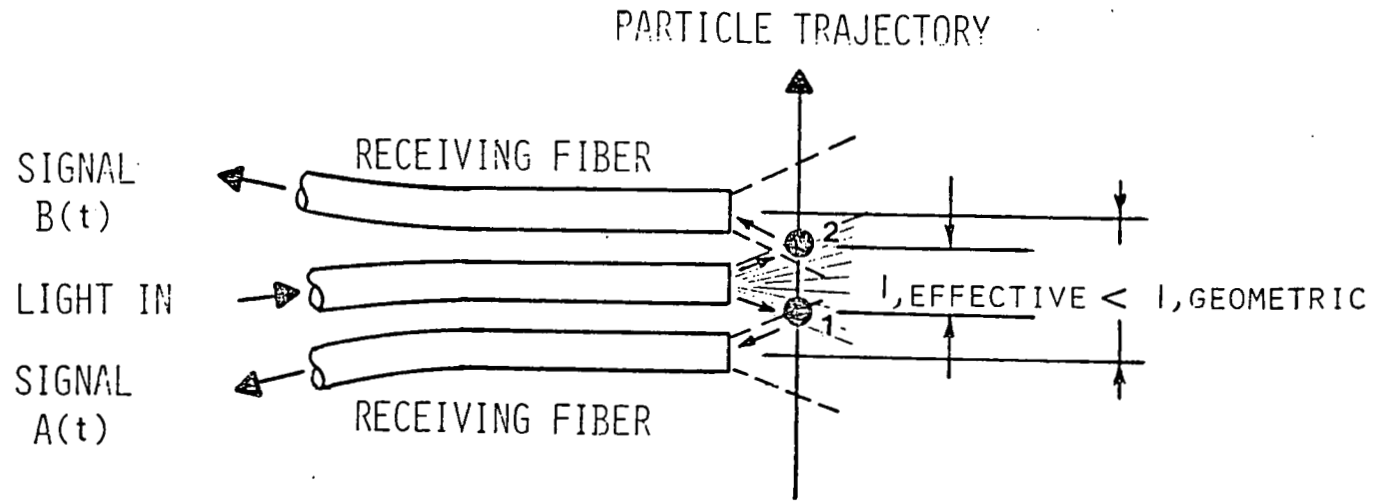

A. CENTRAL ILLUMINATION

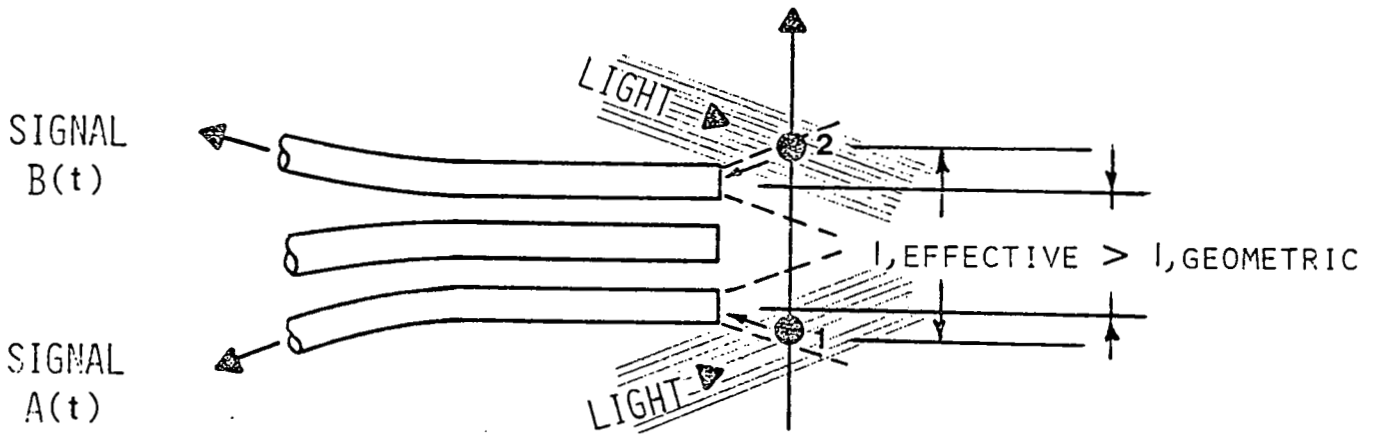

B. EXTERNAL ILLUMINATION

Figure 1.6: Influence of illumination and fiber viewing angle on the effective distance. The shaded area indicates illumination and the dashed lines indicate the viewing angle of the receiving fibers.

Figure 1.6(a) represents the case where only one central fiber is used to illuminate the measuring site. The shaded area indicates the cone of illumination produced in the region immediately in front of the fiber. The dashed lines indicate the angle of vision of the receiving fibers which is a characteristic of the optical fiber. Light from beyond the angle of vision is not captured by the receiving fibers since the angle of incidence is smaller than that required for total internal reflection to occur within the fiber. In Figure 1.6 it can be seen that the bottom fiber receives maximum reflected light from the moving particle when the particle reaches position 1.

Similarly, the top fiber receives maximum reflected light when the particle reaches position 2. Therefore, the delay between maxima will be smaller than that expected if the maximum intensity were to occur when the particle passed over the fiber center. The inverse effect is observed if no light is introduced through the central fiber, and the measuring site is illuminated from beyond the two receiving fibers. The effective distance computed for this case would therefore be greater than the geometric separation distance (Figure 1.6(b)). This was confirmed by experiments done with the same probe ($\ell_{geometric}$ = 0.37 mm) and using two different types of illumination. External illumination gave a computed effective distance of 0.42 mm, and using internal illumination gave an effective distance of 0.14 mm.

If the measuring site is very uniformly illuminated, the computed effective distance would be expected to exactly equal the geometric fiber separation distance. This would also be the case if the viewing angle of the receiving fibers was equal to zero. These effects are currently being investigated using different optical fibers and configurations within the probe. It should, however, be noted that it is of little consequence whether the computed effective distance for a particular probe is equal to or different from its geometric fiber to fiber separation distance. The only requirement is that the probe be calibrated to compute its $\ell_{effective}$, and this value be used for ℓ when computing velocities using Equation (1.2).

EXPERIMENTAL

The particle velocity measurements were carried out in a 305 x 19 mm rectangular cross-sectional bed with transparent Plexiglas walls. The nozzles in the distributor plate were of 19 x 3.2 mm rectangular cross section, spaced 50 mm apart, and had porous packing in them to produce a

uniform distribution of air through the nozzles. Glass beads were used as the bed material (ρ_s = 2470 kg/m^3; $d_{p,avg}$ = 500 μm; 13.2 wt % 710-590 μm, 64.3 wt % 590-420 μm, 22.2 wt % 420-297 μm, 0.3 % < 297 μm).

The air used was prehumidifed to minimize the build up of static charge on the glass beads and the bed walls.

The probe was introduced through a 64 x 50 mm test grid composed of an array of 0.9 mm holes spaced 2.5 mm apart. The grid extended 64 mm above from the top level of the distributor.

Local average particle velocities were measured in this study. Since the receiving fibers are positioned a very short distance apart, a typical particle transit time between these fibers is very small (~ 10^{-4} sec) in comparison to the sampling time of the correlator (~ 10^2 sec). The computed velocity will therefore always be an average over the sampling time (though small). Ishida et al. (1980) have recently reported unsteady state particle velocity measurements using a multifiber optical probe in conjunction with a microcomputer data processor. The signals received by the optical fibers were recorded by an analog data recorder and subsequently processed to compute instantaneous velocities.

MEASUREMENTS IN THE TWO-DIMENSIONAL BED

A. Verification of Two-Dimensional Behavior of the Bed

Particle velocities were measured for a fixed air flow rate at different probe penetrations into the thickness of the bed. If the bed had ideal two-dimensional flow characteristics, there would be no variation across the bed thickness.

Figure 1.7 compares velocities measured at the jet axis with measurements made in the dense phase at the same elevation from the distributor. Figure 1.8 compares velocities along the jet axis at two distances from the nozzle. Velocities measured at the jet axis show variation across the thickness of the bed--indicating non-uniform distribution of air flow through the distributor nozzle. In the dense phase, however, the velocity remains almost unchanged across the bed thickness. The variations caused by the non-uniformity in air flow across the nozzle width therefore die down with increasing lateral distance from the jet axis and also with increasing vertical distance from the nozzle.

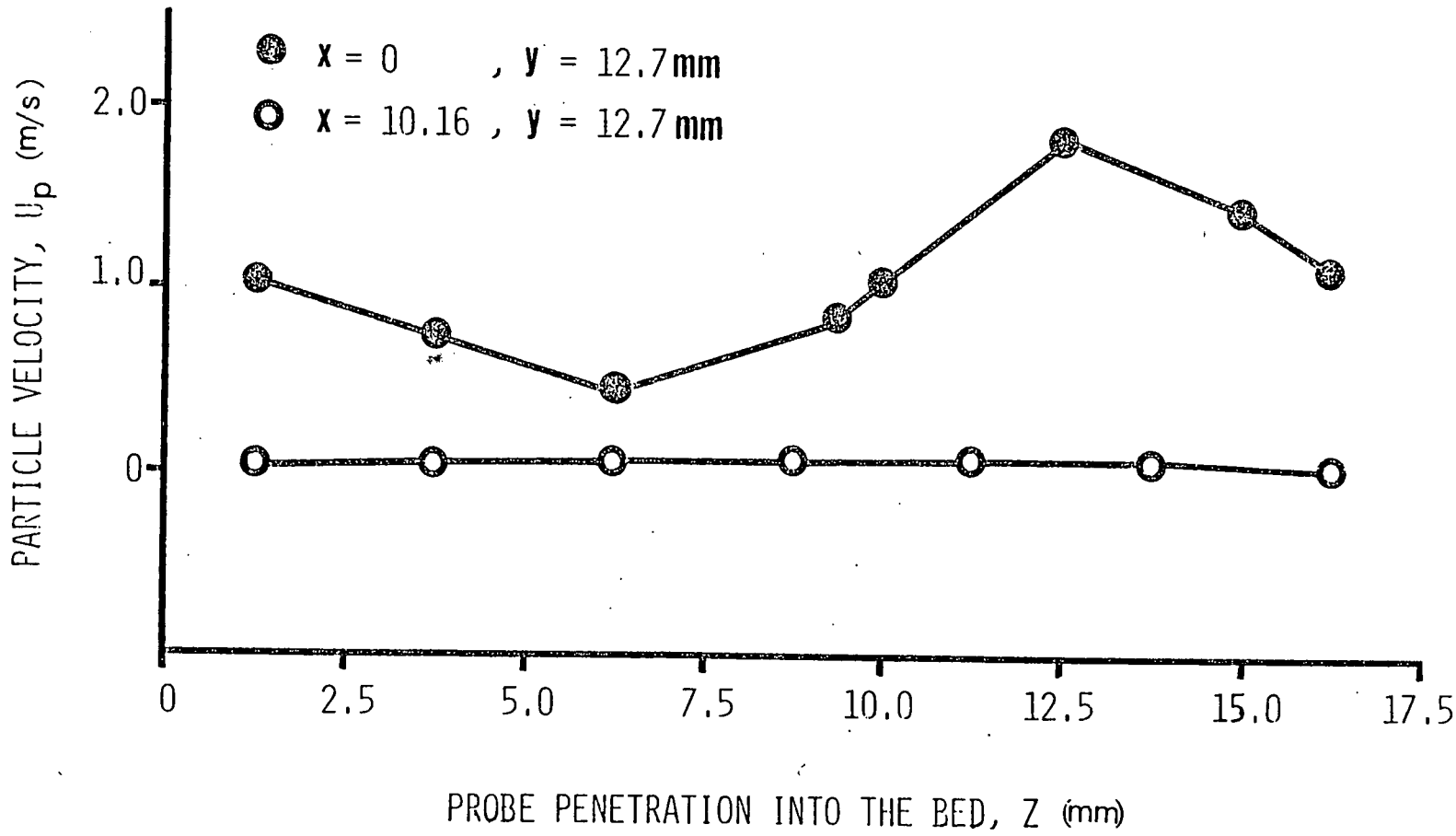

Figure 1.7: Variation of particle velocity along the bed thickness. Verification of two-dimensional nature using the optical fiber probe.

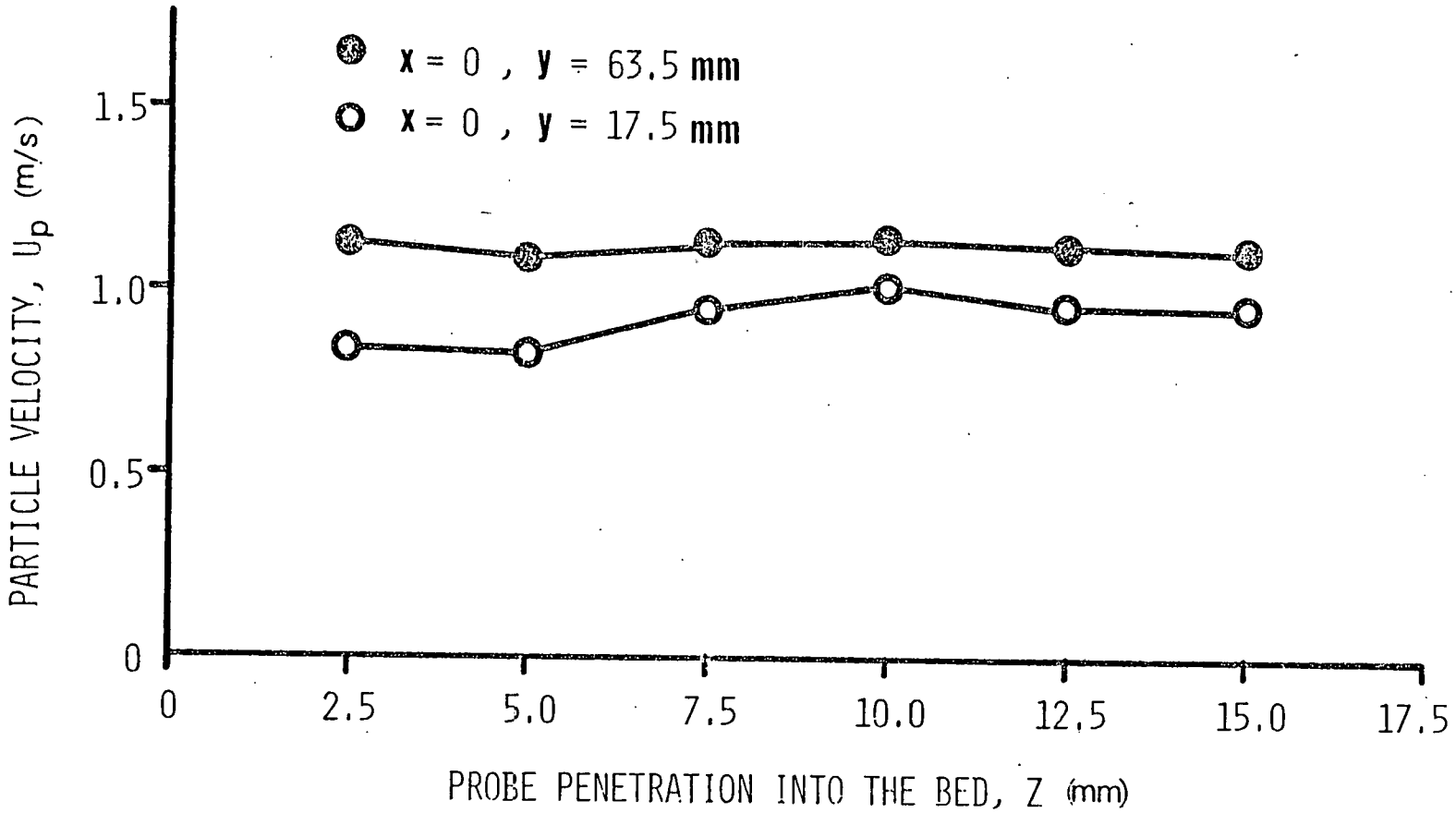

Figure 1.8: Variation of particle velocity along the thickness of the jet. Verification of two-dimensional nature using the LDV.

Based on the observed non-ideal two-dimensional flow characteristics, all other particle velocity measurements were made on the half plane of the bed.

B. Comparison of Probe with LDV Measurements

Particle velocities were measured at corresponding locations within a jet in the two-dimensional bed using the optical fiber probe and a Laser Doppler Velocimeter (LDV) for identical bed and flow conditions. The transparent walls and the two-dimensional geometry of the bed made it possible to use the LDV to measure velocities within the jet. The probe measurements agree well with the LDV results in the main jet region, and are compared in Table 1.2. Such a comparison made in the actual flow itself demonstrated the suitability of the optical fiber probe for particle velocity measurements within fludized beds. It therefore would be possible to measure particle velocities within a three-dimensional bed using an optical fiberprobe, whereas LDV would not be applicable.

C. Bed Fully Penetrated by a Single Jet: Spout Case

The bed was filled with particles to a depth of 43.2 mm. A single jet was created using air flow to only the central nozzle. Keeping the air flow rate constant at 1.7×10^{-3} m^3/s produced a steady jet that fully penetrated the bed. Particle velocities were measured at various points in the bed by inserting the probe through the test holes in the bed wall, after allowing the flow to reach steady state. Figure 1.9 is a particle flow map on which each arrow indicates the direction of the velocity vector computed at that location using the optical fiber probe. The arrows have been joined to indicate possible particle trajectories as solids move downward in the dense region of the bed, are entrained in the jet, and are conveyed vertically upward in the central core. No particle motion was observed in the sheaded dead zones.

Based on the computed particle flow map, the fully penetrated bed may be viewed as composed of three rather distinct regions: a jet core, a narrow jet boundary region, and a packed bed region.

In the jet core region the solids entrained in the jet are pneumatically conveyed upward by the gas. The solid particles are accelerated upward initially and then may attain terminal velocity. Higher up in the 'spout' itself gas and particle velocities decrease and the particles return to the bed.

The major change in direction (downward to upward) of the particles is seen to occur in a very narrow jet

TABLE 1.1: EFFECTIVE DISTANCE COMPUTATION

y location [mm]	LDV measurement U_p [m/s]	Transit time τ_o [s]	Effective distance $\ell = U_p \cdot \tau_o$ [m]
20	0.75	1.95×10^{-4}	1.46×10^{-4}
40	0.91	1.45×10^{-4}	1.32×10^{-4}
60	1.04	1.25×10^{-4}	1.3×10^{-4}
100	1.56	0.95×10^{-4}	1.48×10^{-4}
200	2.33	0.65×10^{-4}	1.51×10^{-4}

TABLE 1.2: COMPARISON OF PARTICLE VELOCITIES MEASURED USING LDV AND THE OPTICAL FIBER PROBE AT CORRESPONDING LOCATIONS IN THE TWO-DIMENSIONAL BED. (h_i = 43.2 mm, $G_o = 2 \times 10^{-3}$ m^3/s.)

Location in the bed (mm)		U_p, LDV (m/s)	U_p, probe (m/s)	% Difference
y	x			
25.4	2.54	0.54	0.56	3.7
40.64	15.24	0.58	0.51	12.0
38.1	0	1.15	1.16	0.9
50.8	0	1.15	1.16	0.9
63.5	0	1.15	1.16	0.9

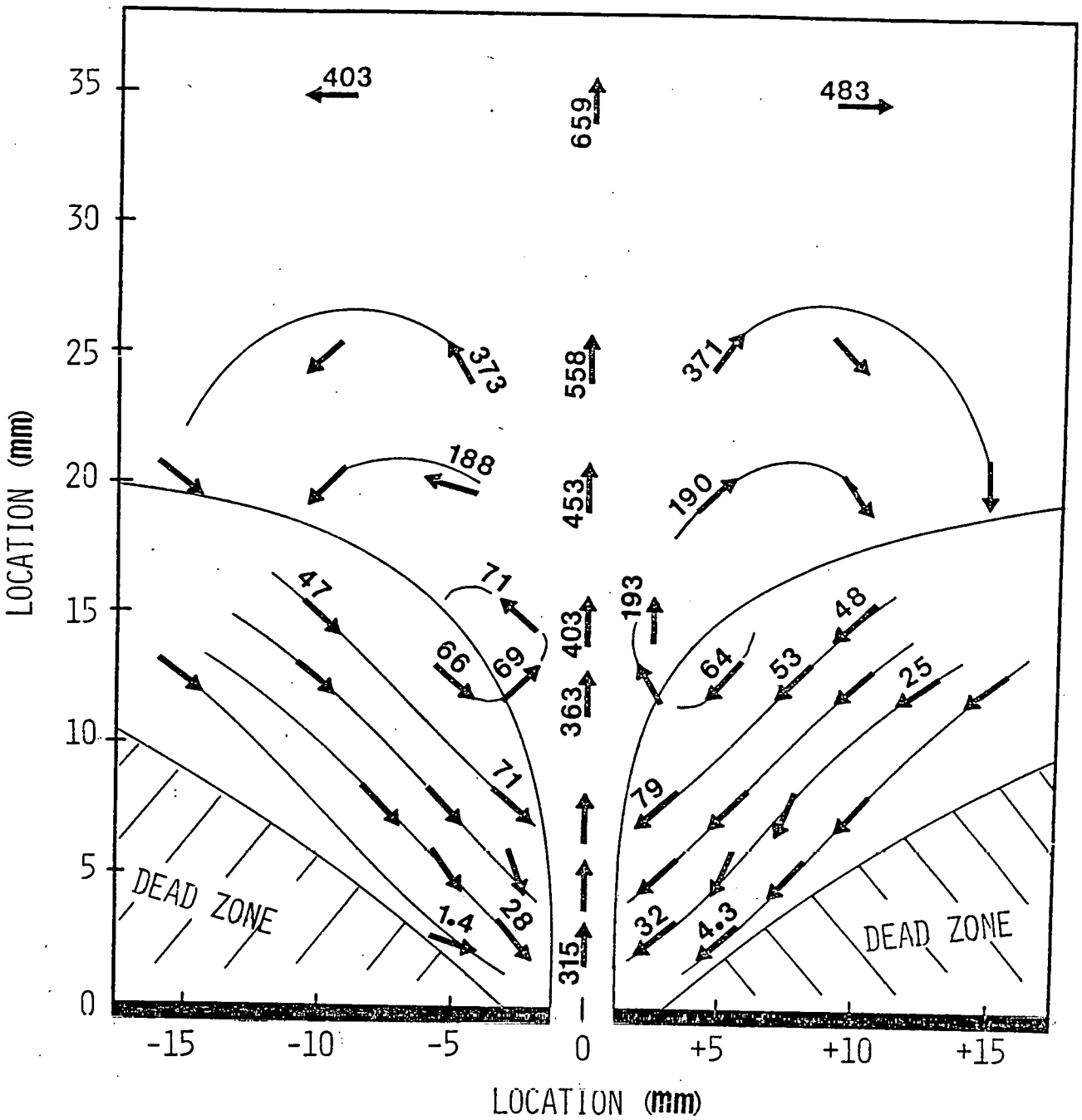

Figure 1.9: Particle flow map of a spouted bed. Velocities indicated in mm/s. (Glass beads, h_i = 43.2 mm, G_o = 1.7 x 10^{-3} m^3/s.)

boundary region. The particles in the packed bed region slide downward toward the jet nozzle and are entrained by the jet when they reach the jet boundary.

D. Bed Fluidized Using Multiple Jets

Initial bed height was 184 mm. The bed was fluidized using equal flow rates of air through each of the five nozzles on the distributor. Particle velocities were measured in the jet and in the region beyond the jet penetration lengths predicted by the correlations of Zenz (1968), Merry (1975), and Yang and Keairns (1978). Beyond the jet penetration length, the jet breaks down into a stream of fast-moving bubbles (Rowe et al., 1979). Particle motion is also rapid in the vicinity of this developing bubble chain and it is not possible from only the velocity measurements to define the point at which the jet breaks down into bubbles. Two different air flow rates were studied and the particle flow maps computed using the optical fiber probe are presented in Figures 1.10 and 1.11.

It has not been possible to compare the particle velocity measurements down here with those reported by Donadono and Massimilla (1978) since this study was performed in a deeper bed using a multiple nozzle arrangement and at much lower nozzle velocities (~ 5 m/s vs. 90 m/s). Their work was done with a single jet fully penetrating a particle bed that was well fluidized using a porous plate distributor. Studies at higher gas velocities and using different distributor configurations are in progress.

CONCLUSIONS AND SIGNIFICANCE

The possibility of measuring solid velocity in the neighborhood of the distributor plate has been demonstrated. The measurements also show that the assumption of two-dimensional behavior in flat beds is valid except in the immediate neighborhood of the grid orifices, since no velocity differences were found across the thickness of the bed. Velocities measuring using the optical fiber probe are presented in flow maps (Figures 1.9-1.11) that indicate solids circulation patterns and stagnant regions formed near the distributor plate.

The transit time correlation approach using the optical fiber probe was found to be a convenient technique to measure particle velocities in two-phase flows with minimal interference to the flow. The technique is easy to apply and does not require prior knowledge of the flow orientation. It also does not require alignment or orientation along the direction of flow as one would when using a pitot tube. Two transit time measurements made 90 degrees apart are sufficient to determine the magnitude and direction of the particle velocity.

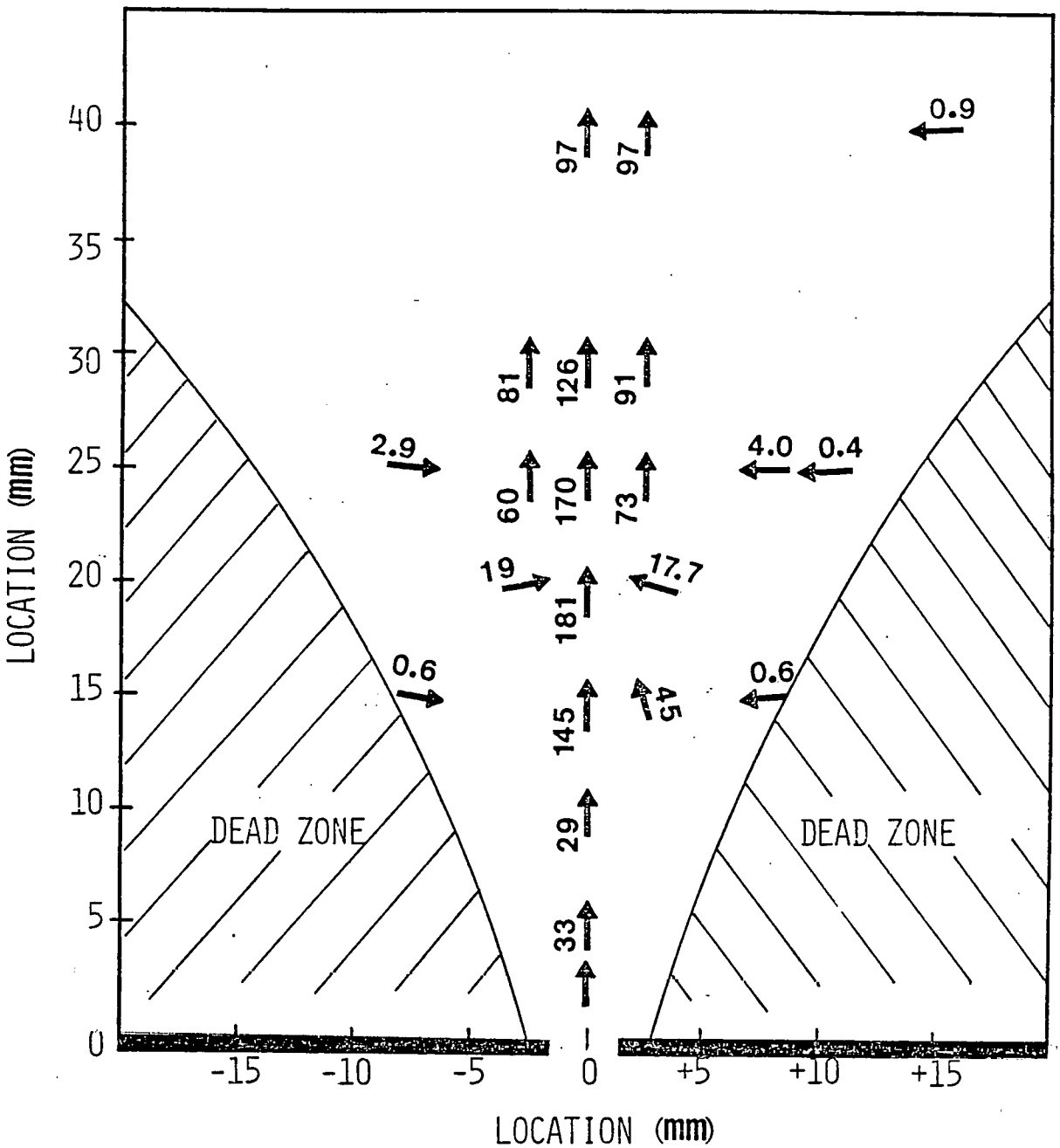

Figure 1.10: Solids circulation around a jet in a bed fluidized using five jets. Velocities indicated in mm/s. (Glass beads, h_i = 184 mm, G_o = 5.2 x 10^{-4} m^3/s.)

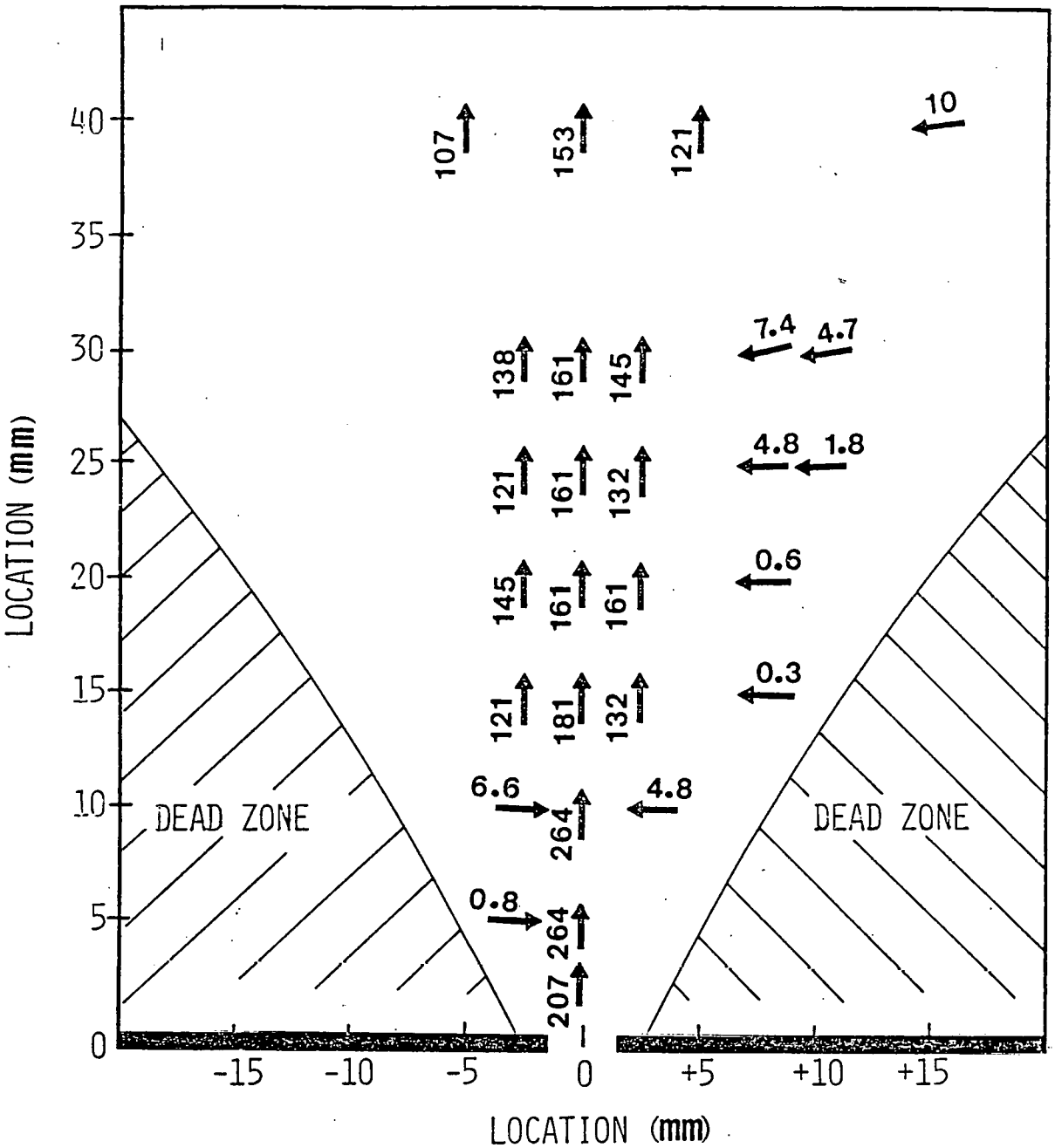

Figure 1.11: Solids circulation around a jet in a bed fluidized using five jets. Velocities indicated in mm/s. (Glass beads, h_i = 184 mm, $G_o = 5.75 \times 10^{-4}$ m^3/s.)

NOMENCLATURE

$A(t)$	signal transmitted by the fiber at point A
$B(t)$	signal transmitted by the fiber at point B
d_p	particle diameter
d_x	component of ℓ_x in the flow direction
d_y	component of ℓ_y in the flow direction
G_o	inlet gas flow rate
h_i	initial bed height
k	a constant
ℓ_{AB}	linear distance between points A and B
ℓ_x	x fiber separation distance
ℓ_y	y fiber separation distance
$N_A(t)$, $N_B(t)$	random noise components
t	time
T	sampling time
U_p	particle velocity
x	lateral distance from the jet axis
y	axial distance from the nozzle
z	probe penetration into the bed thickness

Greek Letters:

τ_o	transit time
Φ_{AB}	cross-correlation function
θ	flow orientation with respect to horizontal
ρ_s	solid density
ε	void fraction

LITERATURE CITED

Beck, M. S., J. Drane, A. Plaskowski, and N. Wainwright, "Particle Velocity and Mass Flow Measurements in Pneumatic Conveyors," Powder Tech., 2, 269 (1968).

Beck, M. S., K. T. Lee, and N. G. Stanley-wood, " A New Method for Evaluating the Size of Solid Particles Flowing in a Turbulent Fluid," Powder Tech., 8, 85 (1973).

Behie, L. A. and P. Kehoe, "The Grid Region in a Fluidized Bed Reactor," AIChE J., 19, 1070 (1973).

Bottom, R. J., "Gas Solid Contacting in Fluidized Beds," Chem. Eng. Prog. Symp. Ser. No. 101, 66, 8 (1970).

Birchenough, A. and J. S. Mason, "Laser Anemometry Measurements in a Gas Solid Suspension Flow," Optics and Laser Tech., 8, 6, 253 (1976).

Cooke, M. J., W. Harris, J. Highley, and D. F. Williams, "Kinetics of Oxygen Consumption in Fluidized Bed Carbonizers," Tripartite Chem. Eng. Conf. Symp. on Fluidization I, p. 14, Montreal (1968).

Donadono, S., A. Maresca, and L. Massimilla, "Gas Injection in Shallow Beds of Fluidized Coarse Solids," Ing. Chim. Ital., 16, 1-2, 1 (1980).

_____ and L. Massimilla, "Mechanics of Momentum and Heat Transfer Between Gas Jets and Fluidized Beds," Fluidization, Cambridge University Press, p. 375 (1978).

Donsi, G., L. Massimilla, and L. Colantuoni, "The Dispersion of Axi-Symmetric Gas Jets in Fluidized Beds," Fluidization, New Hampshire Proceedings, p. 295 (1980).

Heertjes, P. M., J. Verloop, and R. Willems, "The Measurement of Local Mass Flow Rates and Particle Velocities in Fluid-Solid Flows," Powder Tech., 4, 38 (1970).

Hemstrom, G., K. Moller, and B. Norman, "Boundary Layer Studies in Pulp Suspension Flow," 59, 8, 115 (1976).

Ishida, M., T. Shirai, and A. Nishiwaki, "Measurement of the Velocity and Direction of Flow of Solid Particles in a Fluidized Bed," Powder Tech., 27, 1 (1980).

Knowlton, T. M. and I. Hirsam, "The Effect of Pressure on Jet Penetration in Semi-Cylindrical Gas Fluidized Beds," Fluidization, New Hampshire Proceedings, p. 315 (1980).

Latif, B.A.F. and J. F. Richardson, "Circulation Patterns and Velocity Distributions for Particles in a Liquid Fluidized Bed," Chem. Eng. Sci., 27, 1933 (1972).

Lee, S. L. and J. Srinivasan, "LDA Technique Applied to Two-Phase Flow," Two-Phase Flow Instrumentation Review Group Meeting, ONRR/NRC Proceedings, p. I. 4-1 (1977).

Livshits, Y. E. and A. I. Tamarin, "Solid-Phase Velocity Patterns in Free and Constrained Fluidized Beds," J. Eng. Phy., 36, 4, 418 (1979).

Marsheck, R. M. and A. Gomezplata, "Particle Flow Patterns in a Fluidized Bed," AIChE J., 11, 167 (1965).

Merry, J. M. D., "Penetration of Vertical Jets into Fluidized Beds," AIChE J., 21, 507 (1975).

Miller, N. and R. E. Mitchie, "The Development of a Universal Probe for Measurement of Local Voidage in Liquid-Gas Two-Phase Flow Systems," Eleventh National ASME/AIChE Heat Transfer Conf., p. 82, Minneapolis (1969).

Morton, J. B. and W. H. Clark, "Measurement of Two-Point Velocity Correlations in a Pipe Flow Using Laser Anemometers," J. Phy. Ed. Sci. Instrum., 4, 814 (1971).

Oki, K., P. Walawender, and L. T. Fan, "The Measurement of Local Velocity of Solid Particles," Powder Tech., 18, 171 (1977).

_____and T. Shirai, "Particle Velocity in Fluidized Bed," Fluidization Tech. California Proceedings, I, 95 (1975).

Rowe, P. N., H. J. MacGillvray, and D. J. Cheesman, "Gas Discharge from an Orifice into a Gas Fluidized Bed," Trans. Instn. Chem. Engrs., 57, 194 (1979).

Shirai, T., M. Ishida, Y. Ito, N. Inoue, and S. Kobayashi, "Rotation of a Horizontal Disc within an Aerated Particle Bed," J. Chem. Eng. of Japan, 10, 1, 40 (1977).

Wen, C. Y. and S. Dutta, "Research Needs for the Analysis, Design, and Scaleup of Fluidized Beds," AIChE Symp. Ser. No. 161, 73, 1 (1977).

Yang, W. C. and D. L. Keairns, "Design and Operating Parameters for a Fluidized Bed Agglomerating Combustor/ Gasifier," Fluidization, Cambridge University Press, Cambridge, p. 305 (1980).

Yong, J., Y. Zhiqing, Z. Li, and W. Zhanwen, "A Study of Particle Movement in a Gas Fluidized Bed," Fluidization, Cambridge University Press, Cambridge, p. 365 (1980).

Zenz, F. A., "Bubble Formation and Grid Design," Inst. Chem. Eng. Symp. Ser. No. 30, 136 (1968).

CHAPTER 2

MODELING OF A JET IN A FLUIDIZED BED COMBUSTOR

An air jet entering a fluidized bed coal combustor was modeled as a transported bed reactor with solids being entrained along the jet length and conveyed upward Figure 2.1 is a schematic representation of a two-phase jet in the grid region of a two-dimensional fluidized bed of coal particles. The shape of the jet has been approximated to be of uniform rectangular cross section.

Assumptions made for the jet model are:

1. The jet is well mixed radially with plug flow in the axial direction.

2. The solids entrainment flux through the sides of the jet is uniform along its length.

3. The fluidized emulsion surrounding the jet is well mixed.

4. Gas does not enter or leave through the sides of the jet.

5. The gas and solid phases are at steady state with respect to location along the length of the jet. The gas and solid conversions are functions of reactor length and temperature only.

6. The coal particles are assumsed to be spherical and of uniform size.

7. The coal particles are impervious to the reactants. The heterogeneous reactions occur at the surface of the particles.

COMPONENT AND ENERGY BALANCES

We expect the following reactions to occur in the jet:

	REACTION	RATE (k mol/m^3 s)
1.	$2C + O_2 = 2CO$	R_1
2.	$C + CO_2 = 2CO$	R_2
3.	$CO + 1/2\ O_2 = CO_2$	R_3

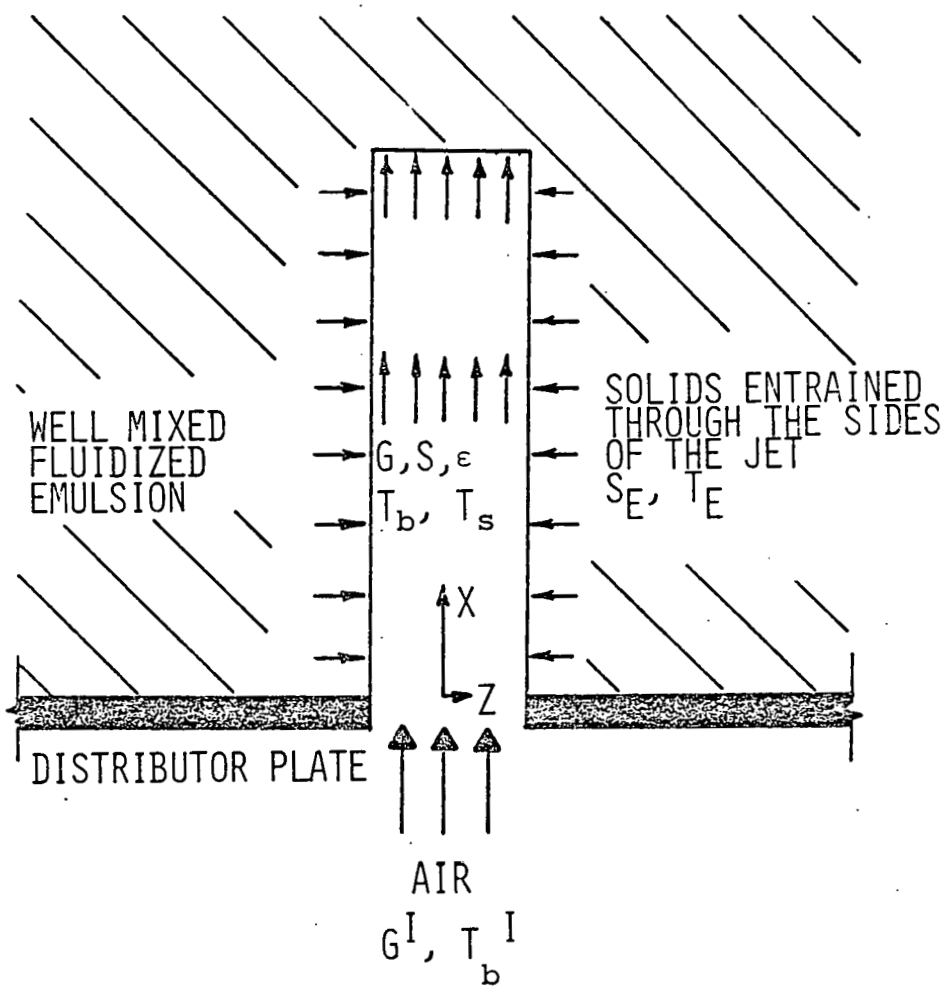

Figure 2.1: The two-phase jet model.

The only linearly independent reactions are

REACTION	RATE (k mol/m^3 s)
1. $2C + O_2 = 2CO$	Z_1
2. $C + CO_2 = 2CO$	Z_2

The rates of production can be expressed as

$$r(O_2) = -Z_1 = -(R_1 + R_3/2)$$

$$r(CO_2) = -Z_2 = -(R_2 + R_3)$$

$$r(CO) = 2(Z_1 + Z_2) = 2(R_1 + R_2) - R_3$$

The differential equations for the oxygen and carbon dioxide mole fractions are

$$G \frac{dy_{O_2}}{dx} = -Z_1 - y_{O_2}(Z_1 + Z_2); \quad y_{O_2} = y_{O_2}^I \quad \text{at } x = 0 \qquad (2.1)\ (2.1a)$$

$$G \frac{dy_{CO_2}}{dx} = -Z_2 - y_{CO_2}(Z_1 + Z_2); \quad y_{CO_2} = y_{CO_2}^I \quad \text{at } x = 0 \qquad (2.2)\ (2.2a)$$

The mole fraction of carbon monoxide is given by

$$y_{CO} = \frac{(1 + y_{CO_2} + y_{O_2})\, y_{CO}^I + 2(y_{O_2}^I - y_{O_2}) + 2(y_{CO_2}^I - y_{CO_2})}{1 + y_{CO_2}^I + y_{O_2}^I} \qquad (2.3)$$

and the total gas flow is obtained from

$$G = G^I (1 + y_{CO_2}^I + y_{O_2}^I)/(1 + y_{CO_2} + y_{O_2}) \qquad (2.4)$$

In all cases the superscript I refers to conditions at the inlet of the jet. The total solids flow at any level is computed using the conservation of the total number of carbon atoms and accounting for the influx of solids through the sides of the jet.

$$S = 2\,S_E\,(x/b) + \frac{G^I\,\{2(y_{O_2}-y_{O_2}{}^I) + (y_{CO_2}-y_{CO_2}{}^I) + y_{O_2}\,y_{CO_2}{}^I - y_{O_2}{}^I\,y_{CO_2}\}}{\{1 + y_{CO_2} + y_{O_2}\}} \quad (2.5)$$

The temperature equations obtained from the gas and solid phase energy balances assuming the temperature of the solid in any cross section to be uniform are

$$S\,C_{ps}\,\frac{dT_s}{dx} = (2R_1+R_2)\,C_{ps}\,(T_s-T_b) - 2S_E\,(L/b)\,C_{ps}\,(T_s-T_E) + R_1(-\Delta H_1)_{T_b} + R_2(-\Delta H_2)_{T_b} + h_p\,a\,(T_b-T_s) \quad (2.6)$$

and

$$(\Sigma_i\,G_i\,C_{pi})\,\frac{dT_b}{dx} = h_p\,a\,(T_s-T_b) + R_3(-\Delta H_3)_{T_b} \quad (2.7)$$

to be solved with initial conditions:

$$T_b = T_b{}^I \qquad \text{at} \qquad x = 0 \quad (2.8)$$

$$T_s = T_E \qquad \text{at} \qquad x = 0 \quad (2.9)$$

To complete the description it is necessary to provide the kinetic information that relates the rates R_1, R_2 and R_3 to the composition and temperature of gas and solid surface.

THE REACTION KINETICS

As a first approximation, the oxygen-carbon and carbon dioxide-carbon reactions are assumed to be first order with respect to the oxygen and carbon dioxide surface concentrations. Further, considering the effect of diffusion in the reaction rate we obtain

$$R_1 = \frac{6\,(1-\varepsilon)}{d_p}\,\frac{k_1\,k_m}{(k_1+k_m)}\,\frac{P}{RT_b}\,y_{O_2,b} \quad (2.10)$$

$$R_2 = \frac{6\,(1-\varepsilon)}{d_p}\,\frac{k_2\,k_m}{(k_1+k_m)}\,\frac{P}{RT_b}\,y_{CO_2,b} \quad (2.11)$$

It is assumed that the particles are spherical of uniform diameter d_p, occupy a fraction $(1-\varepsilon)$ of the reactor volume, and are impervious to the reactants. In addition, the mass transfer coefficient is independent of the species considered and the gases behave ideally. The values reported by Frank-Kamenetskii (1969) were used for the estimation of the rate constants for reactions 1 and 2.

The heat transfer and mass transfer coefficients were estimated using the correlations (Boothroyd, 1971):

$$Nu_p = \frac{h_p d_p}{k_s} = 2 + 0.6\ Re_p^{0.5}\ Pr^{0.3} \tag{2.12}$$

$$Nu_m = \frac{k_m d_p}{D} = 2 + 0.6\ Re_p^{0.5}\ Sc^{0.3} \tag{2.13}$$

The correlation proposed by Howard et al. (1973) was used for the homogeneous gas phase carbon monoxide combustion rate (Reaction 3).

$$R_3 = 1.3 \times 10^{11}\ C_{CO,b} (C_{O_2,b})^{1/2}\ (C_{H_2O,b})^{1/2}\ \exp(-30{,}000/RT_b) \tag{2.14}$$

THE DIMENSIONLESS EQUATIONS

Equations (2.1,2.2,2.6 and 2.7) when integrated with initial conditions (2.1a,2.2a,2.8 and 2.9), using the auxiliary Equations (2.3,2.4 and 2.5) and the kinetic expressions (2.10,2.11 and 2.14), completely describe the variations in temperature and concentration along the jet length.

To minimize the number of parameters involved in the calculation it is convenient to use the dimensionless version of the equations. They are:

$$G^* \frac{dy_{O_2}}{dx} = -\left(R_1^* + \frac{R_3^*}{2}\right) - y_{O_2}\left(R_1^* + R_2^* - \frac{R_3^*}{2}\right) \tag{2.15}$$

$$G^* \frac{dy_{CO_2}}{dx} = -\left(R_2^* - R_3^*\right) - y_{CO_2}\left(R_1^* + R_2^* - \frac{R_3^*}{2}\right) \tag{2.16}$$

$$S^* \beta \frac{dT_s^*}{dx} = R_1^*(-\Delta H_1^*) + R_2(-\Delta H_2^*) + (2R_1^* + R_2^*) \beta (T_s^* - T_b^*)$$

$$- S_E^* \beta (T_s^* - T_E^*) - HA^* (T_s^* - T_b^*) \quad (2.17)$$

$$G^* \frac{dT_b^*}{dx} = R_3^*(-\Delta H_3^*) + HA^* (T_s^* - T_b^*) \quad (2.18)$$

$$Y_{CO_2}(0) = Y_{CO_2}^I, Y_{O_2}(0) = Y_{O_2}^I, T_b^*(0) = 1, T_s^*(0) = T_s^I/T_b^I \quad (2.18a)$$

and the auxiliary equations

$$G^* = (1 + Y_{CO_2}^I + Y_{O_2}^I)/(1 + Y_{CO}^2 + Y_{O_2}) \quad (2.19)$$

and

$$S^* = S_E^* X + \frac{2(Y_{O_2} - Y_{O_2}^I) + (Y_{CO_2} - Y_{CO_2}^I) + Y_{O_2} Y_{CO_2}^I - Y_{O_2}^I Y_{CO_2}}{(1 + Y_{CO_2} + Y_{O_2})} \quad (2.20)$$

The dimensionless variables and parameters used are defined below:

$G^* = G/G^I$, $T_b^* = T_b/T_b^I$

$S^* = S/G^I$, $T_s^* = T_s/T_b^I$

$S_E^* = 2 S_E L/b G^I$, $T_E^* = T_E/T_b^I$

$R_i^* = R_i L/G^I$, $\Delta H_i^* = \Delta H_i/C_{pg} T_b^I$

$X = x/L$, $HA^* = h_p a L/G^I C_{pg}$

$\beta = C_{ps}/C_{pg}$

SIMULATION RESULTS

Operating conditions similar to those that are to be expected in a jet entering a fluidized bed combustor were chosen. Values for gas inlet velocity and mass flow rates of entrained particles in the jet were obtained from the measurements reported by Donadono and Massimilla (1978). These values were converted into an equivalent solids entrainment flux through the sides of a jet. Conditions used for the simulation are summarized below:

Length of jet	1 m
Jet cross section	0.005 x 0.02 m
Char particle size	200 m
Char composition (wt %)	1% C + 99% inert.
Gas inlet velocity	90 m/s
Gas inlet composition	21% O_2 + 79% N_2
Gas inlet temperature	298 K, 523 K
Pressure	2 atm
Solids entrainment flux	2.0, 3.78, 6.0 k mol/m^2 s
Bed temperature	1073 K

The entering gas is heated by the hot bed solids as they are entrained into the jet. Gas and solid temperature profiles along the jet length are shown in Figures 2.2 and 2.3. These results indicate that for the operating conditions chosen, no ignition is to be expected in the jet.

For the simulation conditions chosen here, the correlation of Merry (1975) predicts a jet penetration length of ~ 0.1 m. Beyond the jet penetration length the jet breaks down into a stream of fast-moving bubbles (Rowe et al., 1979). However, this entire region defined by the permanent jet together with the rapidly rising bubbles displays 'jet-like' behavior in that solids are entrained through the sides of this region and are conveyed upward by the rising gas. The model does not attempt to define the point at which the jet breaks down into bubbles, and the simulation is extended to axial distances beyond the 'jet-penetration length.'

Figure 2.2 indicates the relative variation of solids temperature for different entrainment rates through the sides of the jet. Solids at a bed temperature of 1073 K are entrained into the jet and heat the entering gas that is at a lower temperature. The initial drop in solids

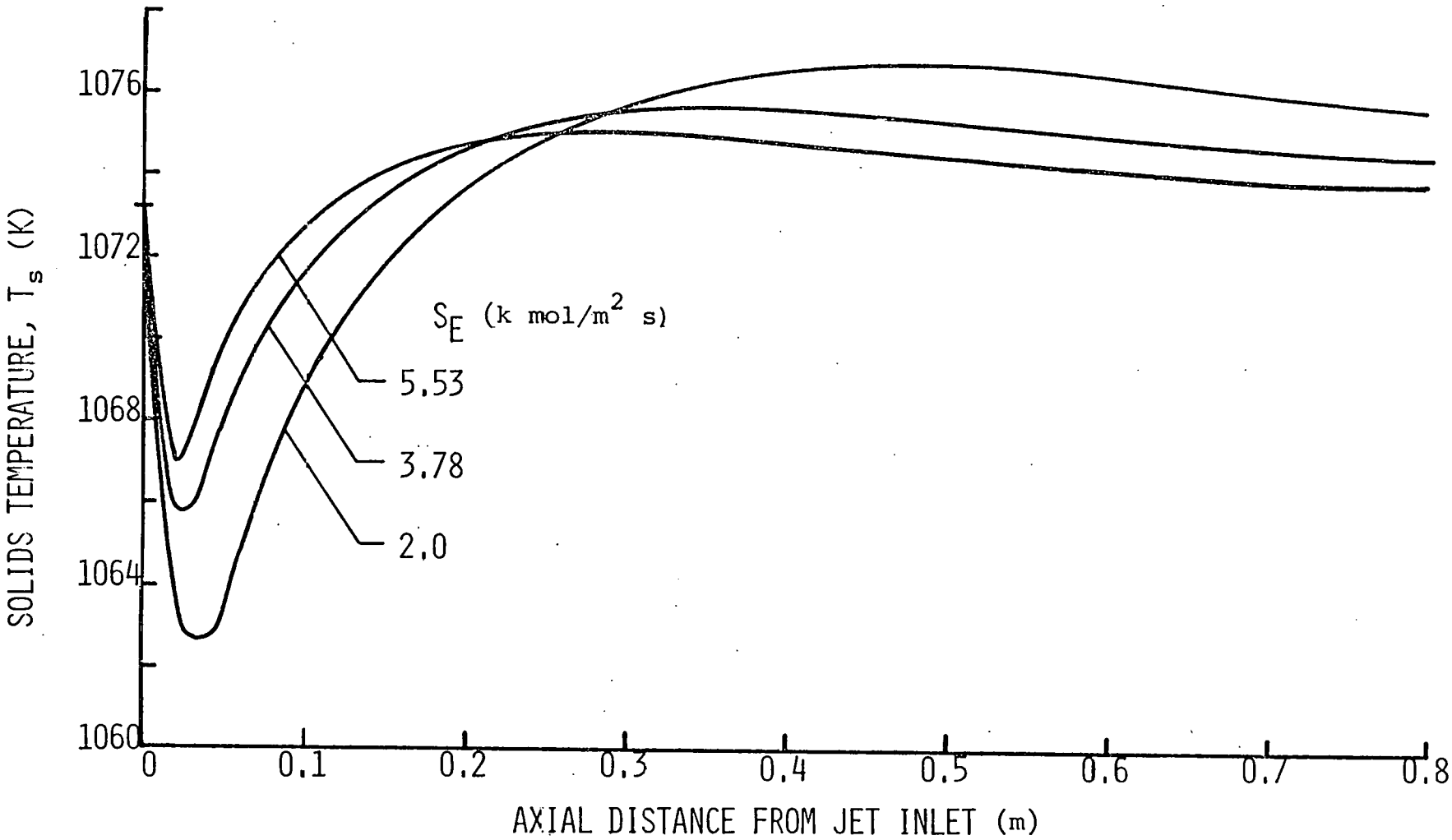

Figure 2.2: Axial variation of solids temperature within the jet for different entrainment rates. (T_E = 1073 K, T_b^I = 523 K.)

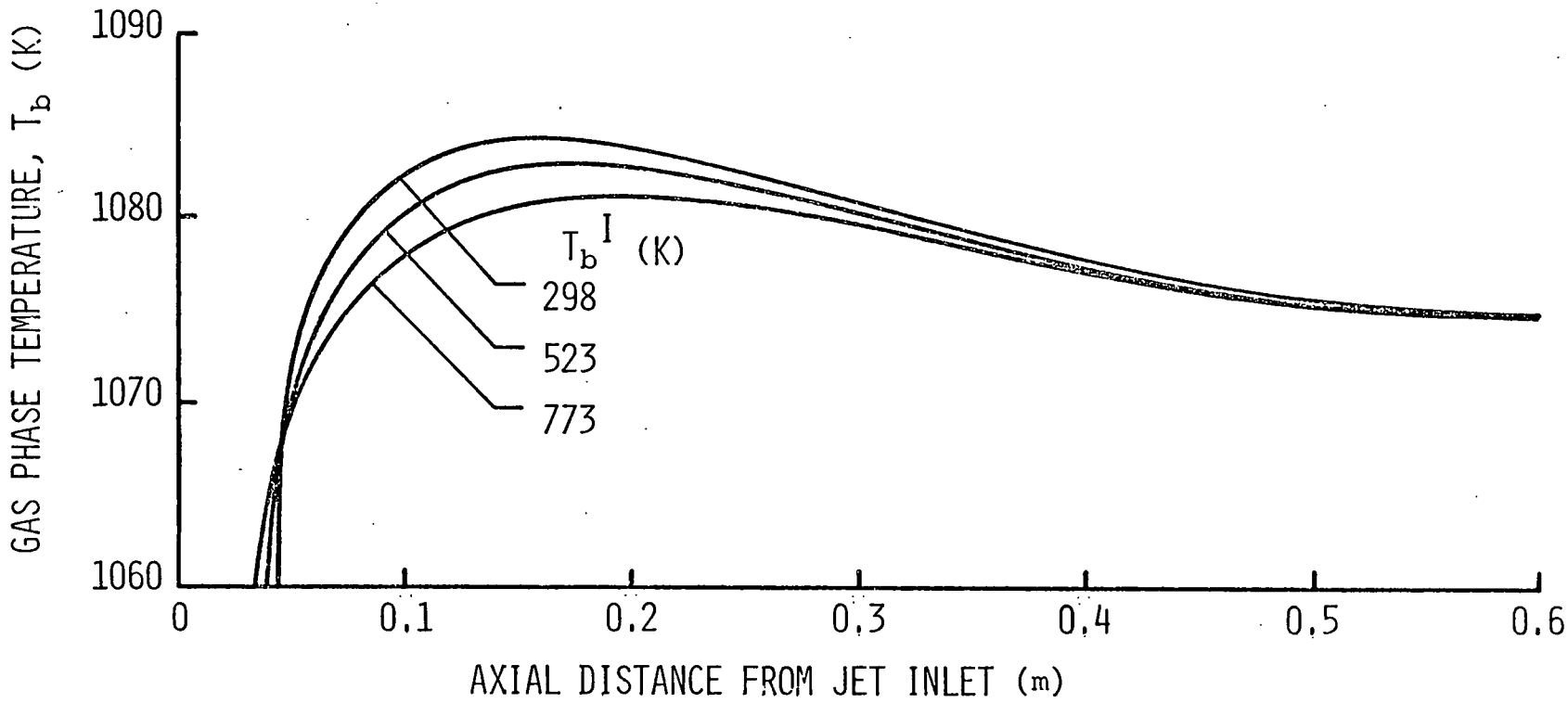

Figure 2.3: Axial variation of gas temperature within the jet for different inlet gas temperatures. (S_E = 3.78 k mol/m^2 s, T_E = 1073 K.)

temperature is due to this heat transfer to the gas phase. The influence of the exothermic surface reaction (1) begins to be seen after the first 3% of the reactor length, causing the solids temperature to recover and rise. The heat transfer effects can be seen as more pronounced in the case of lowest solids entrainment.

Figures 2.4 and 2.5 show the effects of inlet gas temperatures and solids entrainment rates on fractional carbon conversion in the jet. The fractional carbon conversion at any distance x being defined as the (mass of carbon reacted)/(total mass of carbon that has entered the jet in a distance x). The variation in gas composition along the jet axis, for different inlet gas temperatures, is shown in Figure 2.6. Using ambient air (298 K) would result in faster and higher conversion of carbon to carbon dioxide than the use of preheated air. Figure 2.6 indicates that it would be of no use to preheat the air entering the combustor since it would only result in an increased production of carbon monoxide.

The cases studied indicate that considerable reaction occurs in each gas jet entering a fluidized bed coal combustor. Further, the solids entrainment rates encountered are high enough to consume all the oxygen in the entering air and absorb the heat released, so that no ignition is to be expected in the jet region.

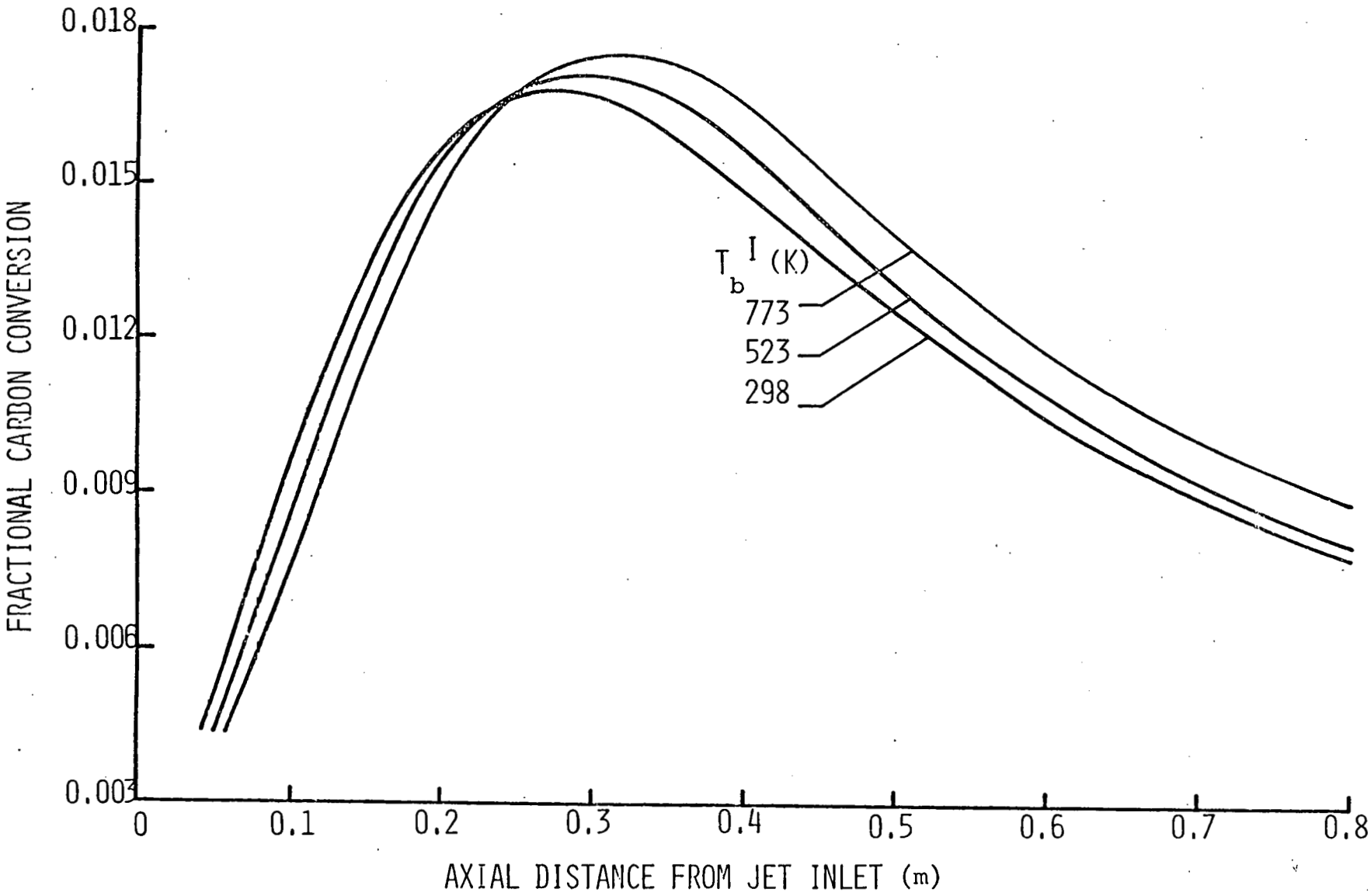

Figure 2.4: Fractional carbon conversion for different inlet gas temperatures. (S_E = 3.78 k mol/m^2 s, T_E = 1073 K.)

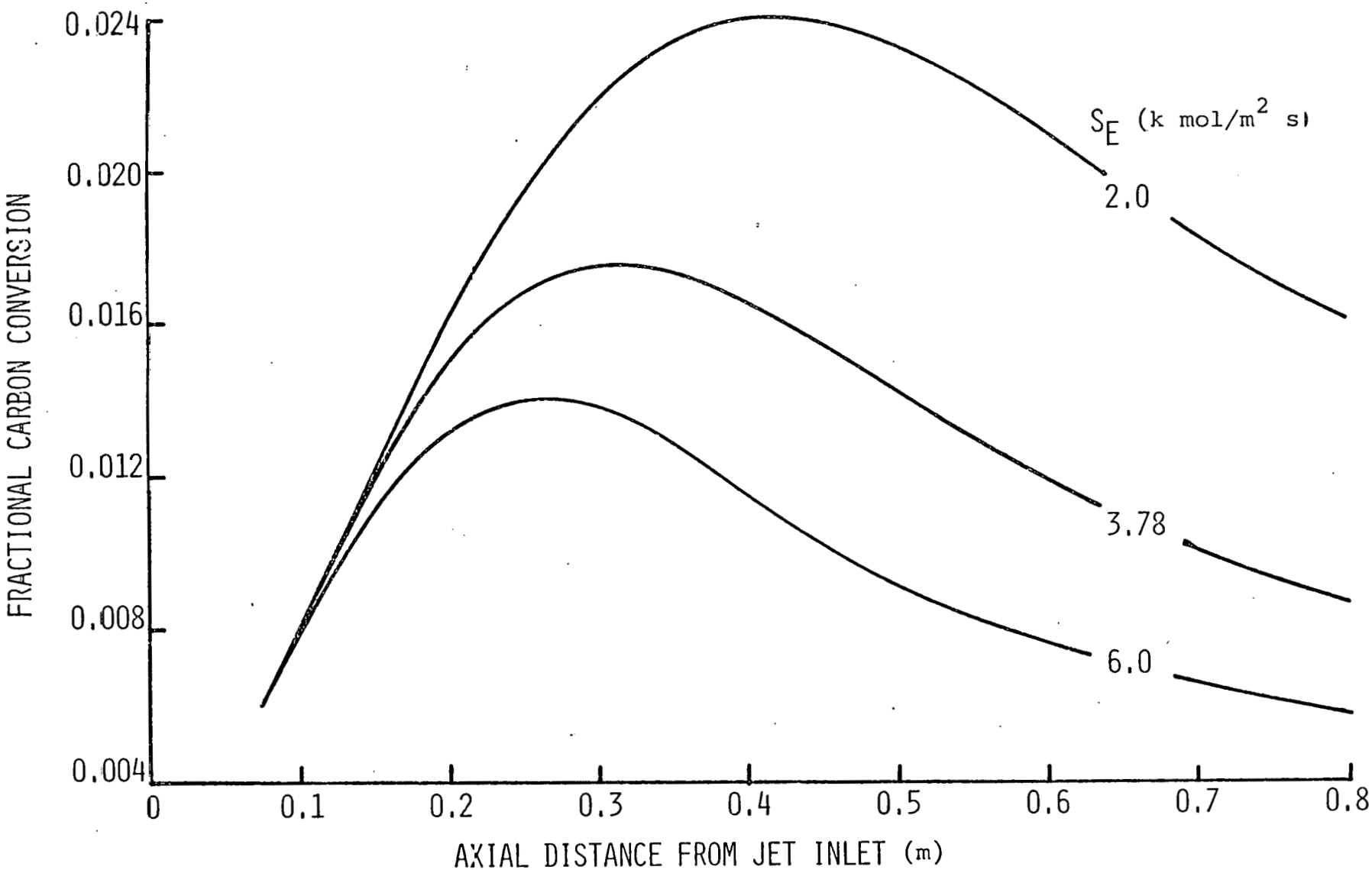

Figure 2.5: Fractional carbon conversion for different solids entrainment rates. (T_E = 1073 K, T_b^I = 773 K.)

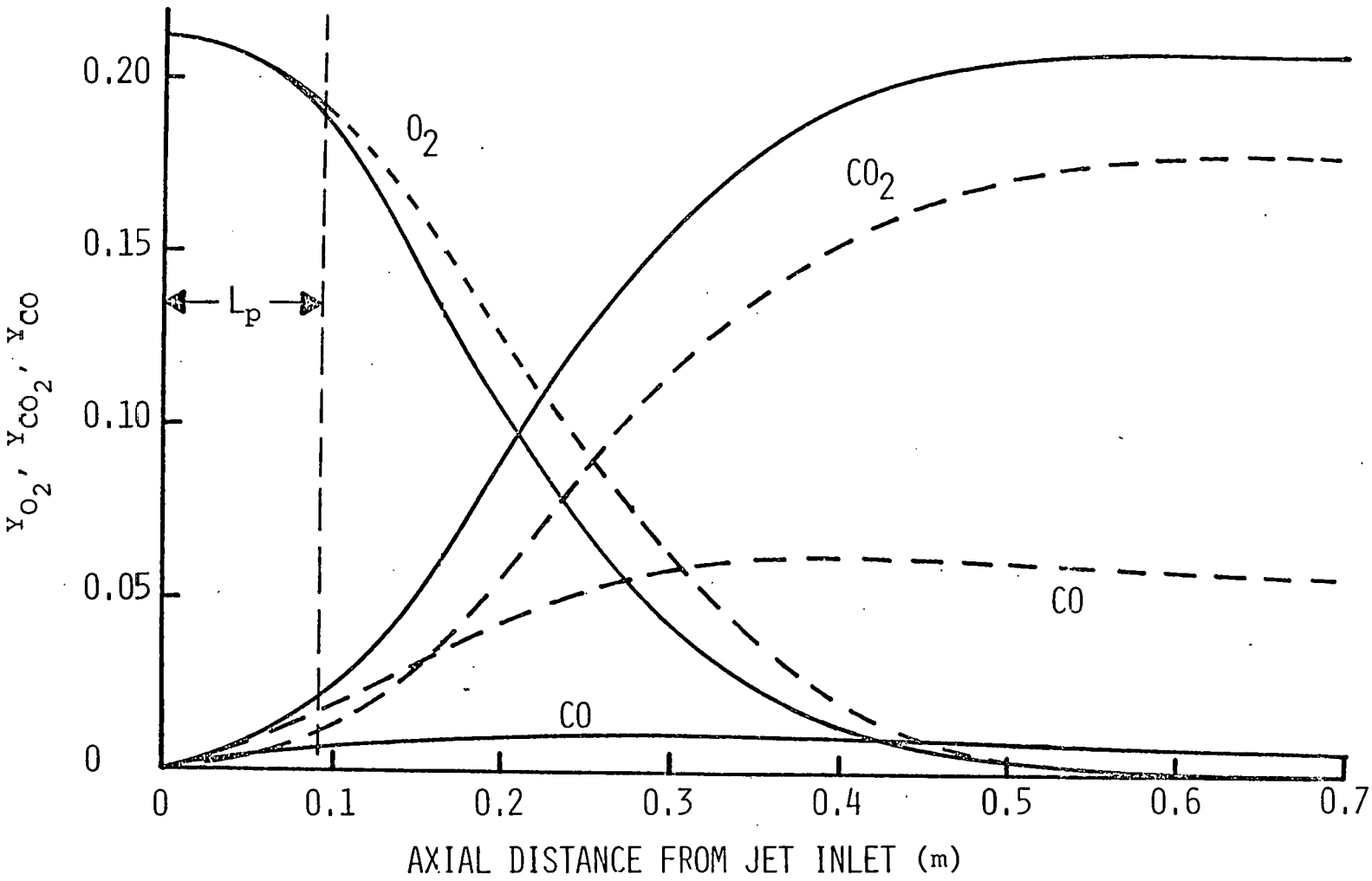

Figure 2.6: Axial variation of gas composition within the jet for different inlet gas temperatures. (—— T_b^I = 298 K, – – – T_b^I = 773 K, S_E = 3.78 k mol/m^2 s, gas composition = 0_2+CO_2+CO+N_2.)

NOMENCLATURE FOR THE JET MODEL

a	surface area of char particles per unit lift tube volume, m^2/m^3
b	jet width, m
$C_{j,b}$	concentration of component j in the bulk phase, moles/m^3
$C_{j,s}$	concentration of component j on the solid surface, moles/m^3
C_{ps}	specific heat of the solid, cal/g mol K
C_{pg}	specific heat of the gas, cal/g mol K
d_p	diameter of char particle, m
D	diffusivity, m^2/s
G	total gas flow per unit cross-sectional area, k mol/m^2 s
h_p	particle heat transfer coefficient, k cal/m^2 s K
k_1, k_2	rate constants for Reactions 1 and 2, m/s
k_f	thermal conductivity of the fluid, k cal/m s K
k_m	mass transfer coefficient, m/s
L	reactor length, m
L_p	jet penetration length, m
Nu	Nusselt number
P	pressure, atm
$r_{s,i}$	rate of surface reaction i, k mol/m^2 s
R	gas constant, m^3 atm/k mol K
Re	Reynolds number

R_i	rate of the i^{th} reaction, k mol/m^3 s
S	total solids flow per unit cross-sectional area, k mol/m^2 s
S_E	solid entrainment flux through the sides of the jet, k mol/m^2 s
T_b	temperature of the gas phase, K
T_E	temperature of the emulsion surrounding the jet, K
T_s	temperature of the char solid, K
x	distance along the jet axis, m
y_j	mole fraction of component j
Z	lateral distance from the jet axis, m
Z_i	specific reaction rate of the i^{th} reaction, k mol/m^3 s
$(-\Delta H_i)$	heat of reaction for the i^{th} reaction, k cal/kg mol
ε	void fraction

Superscript

I	conditions at the bottom of the jet

LITERATURE CITED

Donadono, S. and L. Massimilla, "Mechanisms of Momentum and Heat Transfer between Gas Jets and Fluidized Beds," Fluidization, Cambridge University Press, 1978.

Frank-Kamenetskii, D. A., "Diffusion and Heat Transfer in Chemical Kinetics," Plenum Press, New York, 1969.

Merry, J. M. D., "Penetration of Vertical Jets into Fluidized Beds," AIChE J., 21, 507 (1975).

RECEIVED BY T.C. MAY 15 1987

By MISTARE